All-fiber temporal photonic fractional Hilbert transformer based on a directly designed fiber Bragg grating

Ming Li and Jianping Yao*

*Microwave Photonics Research Laboratory, School of Information Technology and Engineering,
University of Ottawa, Ottawa, Ontario K1N 6N5, Canada*
*Corresponding author: jpyao@site.uottawa.ca

An all-fiber temporal photonic fractional Hilbert transform (FHT) based on a fiber Bragg grating (FBG) is proposed and investigated, for the first time to our knowledge. The photonic FHT is designed based on the discrete layer peeling method, which enables the FBG to have a strong strength. Numerical results show that the FBG can be used to efficiently and accurately implement broadband all-optical FHT for an arbitrary optical waveform with a bandwidth up to hundreds of gigahertz. © 2010 Optical Society of America
OCIS codes: 070.0070, 070.1170, 320.7085.

The temporal Hilbert transform is an important tool for signal processing that can find important applications, such as in modern radar and communications systems [1]. The Hilbert transform (HT) is usually implemented in the electrical domain using digital electronics, but the processing speed is slow owing to the limited sampling speed of the state-of-the-art digital circuits. Thanks to the inherent high speed and large bandwidth offered by optics, the HT can also be implemented in the optical domain with a much higher speed and greater bandwidth [2,3]. Over the past few years, several implementations of the HT in the optical domain have been reported [4–7]. In general, a photonic-assisted HT can be realized based on a multitap photonic transversal filter [4–6] and a fiber Bragg grating (FBG) [7,8]. Emami *et al.* proposed to use a photonic transversal filter to implement the HT, which has been employed to measure the frequency and power of an rf signal [4,5]. The realized HT based on a photonic transversal filter can also be used to implement optical single-sideband (SSB) modulation [6]. In 2006, Hanawa *et al.* proposed to use a sampled FBG as a multitap photonic transversal filter to implement the photonic HT [7]. Very recently, Asghari *et al.* proposed to implement the HT using a uniform weak-coupling FBG with a π phase shift in the FBG [8]. The limitation of this technique is that the FBG should be weak enough to satisfy the Born approximation of the synthesis approach that is based on space-to-frequency-to-time mapping (SFTM) [9], making the FBG very weak.

On the other hand, the classic HT can be generalized with better performance and higher flexibility. A generalized HT is usually called fractional Hilbert transform (FHT) [10]. In an FHT, the transfer function is defined as $H_{FHT}(\omega) = \exp(iP\pi/2)S(\omega) + \exp(-iP\pi/2)S(-\omega)$, where ω is the angular frequency relative to the optical carrier frequency, $S(\omega)$ is the step function, and the parameter P is the fractional order of the FHT. The FHT has been widely employed for signal processing [11]. The implementation proposed in [10] could be realized based on free-

space optics, which can be used for two-dimensional signal processing, such as image processing and pattern recognition; for temporal signal processing, however, a one-dimensional FHT should be employed. In this Letter, we propose, for the first time to the best of our knowledge, an all-fiber photonic FHT based on an FBG. The FBG is directly designed based on the target response in the frequency domain by the discrete-layer-peeling (DLP) method. The key significance of using the DLP method over the SFTM for the FBG design is that the designed FBG is enabled to have a high strength [12,13], which is essential for optical signal processing to ensure a good signal-to-noise ratio.

When an optical signal $x(t)e^{j\omega_0 t}$ is introduced into a classic photonic HT, the output signal $y(t)e^{j\omega_0 t}$ from the photonic HT is given by $y(t) = 1/\pi \mathrm{PV}\int_{-\infty}^{\infty} x(\tau)/(t-\tau)\mathrm{d}\tau$, where $x(t)$ and $y(t)$ are the complex temporal envelopes of the input and output optical signals, respectively; ω_0 is the angular frequency of the optical carrier, and PV is the Cauchy principal value [1]. By applying the Fourier transform to both sides of the expression $y(t)$, we have $Y(\omega) = X(\omega)[-j \operatorname{sgn}(\omega)]$, where $X(\omega)$ is the Fourier transform of the input optical signal, $Y(\omega)$ is the Hilbert-transformed optical signal, and $\operatorname{sgn}(\omega)$ is a sign function (-1 for $\omega < 0$, 0 for $\omega = 0$, and 1 for $\omega > 0$).

As can be seen the transfer function $H_{HT}(\omega)$ of the classic HT is $-j \operatorname{sgn}(\omega)$. For a photonic FHT, the transfer function $H_{FHT}(\omega)$ in the frequency domain is given as [11]

$$H_{FHT}(\omega) = \cos \varphi + \sin(\varphi) \times [-j \operatorname{sgn}(\omega)]$$
$$= \begin{cases} e^{-j\varphi}, & \omega > 0 \\ 0, & \omega = 0 \\ e^{j\varphi}, & \omega < 0 \end{cases}, \qquad (1)$$

where $\varphi = P \times \pi/2$ denotes the phase and P is the fractional order. It can be seen from Eq. (1) that the photonic FHT becomes a classic photonic HT when $P = 1$.

For $P=0$ or $P=2$, we have $H_{\mathrm{FHT}}(\omega)=1$, which means that the fractional Hilbert-transformed signal is identical to the input signal. For $0<P<1$ or $1<P<2$, the output is a weighted sum of the original signal and its classic HT.

Figure 1 shows the magnitude and phase responses of an ideal (solid line) and a practically realizable (dotted line) photonic FHT. The magnitude spectrum of the ideal FHT is kept constant for all the angular frequency, while the phase response has a 2φ phase shift at the central frequency. Since the ideal magnitude response is equal to 1 and extends to infinity, an FBG with such an ideal magnitude response is not practically realizable. To synthesize a practically realizable FBG, the bandwidth $\Delta\omega$ of the magnitude response should be a finite number, as is shown in Fig. 1. Based on the target magnitude response in Fig. 1, an FBG is designed. The design is realized by using the DLP method, which was proposed by Feced and Skaar for the synthesis of an FBG that is able to efficiently and accurately reconstruct the grating structure from any given reflection spectrum [12,13]. Specifically, the target reflection spectrum $r(\omega)$ of the photonic FHT is given,

$$r(\omega)=R\,\exp\left\{-\ln 2\left[\frac{\omega}{0.5\,\omega_{\mathrm{FWHM}}}\right]^{m}\right\}\exp[j\phi(\omega)],\tag{2}$$

where R is the reflectivity, ω_{FWHM} is the FWHM of the magnitude response that has a shape as an mth-order Gaussian function, and $\phi(\omega)$ is the phase response, where $\phi(\omega)=\varphi\,\mathrm{sgn}(-\omega)$.

In the design of the photonic FHT, the reflectivity R is set at 90%, and the FWHM of the magnitude response is 120 GHz, which has the shape of a 16th-order Gaussian function. The phase shift φ is selected to be $\pi/4$, and the central frequency is 192.93 THz (i.e., 1555 nm). Figure 2(a) shows the reflectivity and phase response of the designed photonic FHT based on a 3 cm multiple-phase-shifted uniform FBG. As shown in Fig. 2, the FWHM of the reflectivity spectrum is 120 GHz. There also exists a narrow notch at the central frequency, as shown in the inset of Fig. 2. The notch is formed because of the $\pi/2$ phase shift at
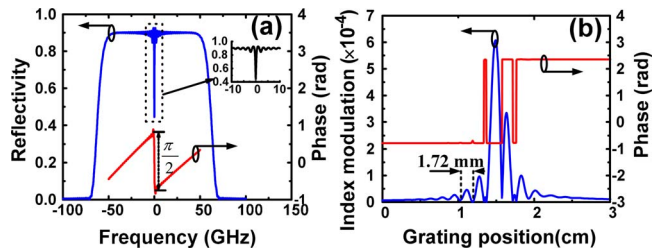
Fig. 2. (Color online) (a) Magnitude and phase responses of the designed photonic FHT based on a 3 cm multiple-phase-shifted FBG; (b) the index modulation and phase profile of the designed photonic FHT.

the central frequency. For a classic photonic HT, the notch depth will be the highest, since the phase shift is π [8]. A nonzero slope of the phase profile is also observed that is caused by a linear phase change due to a constant time delay. Figure 2(b) shows the index modulation and phase profile of the FBG. The zero-to-zero width of the sidelobes in the apodization profile is about 1.72 mm, which is determined by the bandwidth of the reflection spectrum. The maximum index modulation is about 6.07×10^{-4}. For a uniform FBG, a squarelike response in the frequency domain corresponds to a sinc-like index modulation profile. Therefore the multiple π phase shifts in the phase profile of the designed FBG are caused by the squarelike 16th-order Gaussian magnitude spectrum. In the fabrication of the designed FBG, the apodization can be obtained by dephasing the subsequent exposures, while the UV beam scans the phase mask with a technique similar to that reported in [14]. In addition, the maximum index modulation of 6.07×10^{-4} can be realized in a hydrogen-loaded single-mode fiber. Moreover, since the width of the sidelobes is about 1.72 mm, an effective resolution of the writing-beam position control in a range of tens of micrometers will be enough to control the index profile in the fabrication of the FBG. Therefore the designed FBG can be practically fabricated, and the proposed solution is feasible.

To verify the operation of the designed photonic FHT, the temporal response is evaluated by introducing two different input signals to the designed FBG. The central frequencies of the two input signals are both at 192.93 THz. In the first example, as shown in Fig. 3(a), the input signal is a first-order Hermite–Gaussian pulse that is a first-order derivative of a transform-limited 10 ps Gaussian pulse. The output signals reflected from the designed FHT based on the DLP and SFTM methods and based on an ideal FHT are also shown in Fig. 3(a). As can be seen, the output signal reflected from the FBG is close to that obtained by an ideal FHT. The normalized rms error (NRMSE) is smaller than 0.5%. It can also be seen the output signal is asymmetrical with respect to the central frequency, with the right sidelobe being obviously enhanced. As a comparison, the output signal reflected from a photonic FHT designed based on the SFTM is also shown in Fig. 3(a). A relatively large deviation from the ideal output can be obviously observed from the zoom-in view. The deviation is caused by the intrinsic limitation of the SFTM, which
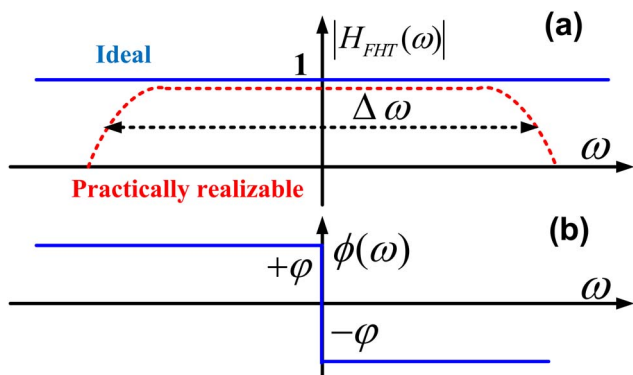

Fig. 1. (Color online) Schematic diagram showing the (a) magnitude response and (b) phase response of an ideal (solid lines) and a practically realizable (dotted lines) photonic FHT.
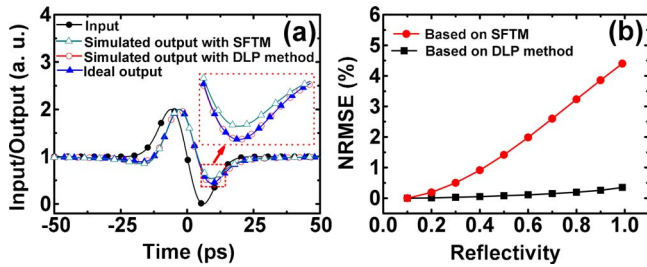
Fig. 3. (Color online) (a) Numerical results for the photonic FHTs designed based on the DLP and SFTM methods and based on an ideal FHT when the input is a first-order Hermite–Gaussian pulse. (b) NRMSEs of the PHTs based on the DLP and SFTM methods for different reflectivities.

requires the FBG to be weak enough to satisfy the Born approximation. Figure 3(b) illustrates the NRMSEs of the PHTs based on the DLP and SFTM methods for different reflectivities (i.e., corresponding to different FBG strengths). It can be seen that the NRMSE based on the SFTM is largely increased along with the increase of the reflectivity. On the other hand, the NRMSE based on the DLP method is kept lower than 0.5%. Therefore the key advantage of using the DLP method for the FBG design is that the FBG can have a strong strength while keeping a very small NRMSE.

To further investigate the side enhancement, in the second example a squarelike 10th-order Gaussian pulse is directed into a photonic FHT, with the fractional order set at four different values. As shown in Fig. 4, all the simulated output waveforms (solid line)

agree very well with the ideally Hilbert-transformed waveforms (dotted line). For $P=2$, the output waveform is identical to the input signal. The output waveform for $P=0.5$ is right-side enhanced, and the side enhancement is reversed for $P=1.5$. In addition, for $P=1$, the left and right sides of the output waveform become symmetrical. This property can be used to enhance either the ascend side or the descend side of an input optical pulse by giving a different fractional order. The proposed photonic FHT can also be used to construct a broadband and ultrafast secure SSB modulation by taking the fractional order as a secret key [11].

In summary, we have proposed an FBG-based temporal photonic FHT that can be used to process an ultrafast and broadband microwave signal. The key device was the FBG, which was directly designed by the DLP method. The key advantage of using the DLP method for the FBG design is that the FBG can have a high strength, which is important in signal processing where a good signal-to-noise ratio at the output of the processor is always expected. In addition, the use of the DLP method also provides the flexibility in designing a photonic FHT with an arbitrary bandwidth and arbitrary fractional order. The designed FBG was uniform in period with a few π phase shifts, which could be fabricated using a phase-mask-based fabrication system by laterally shifting the phase mask with a high-precision piezo motor to introduce the π phase shifts [14].
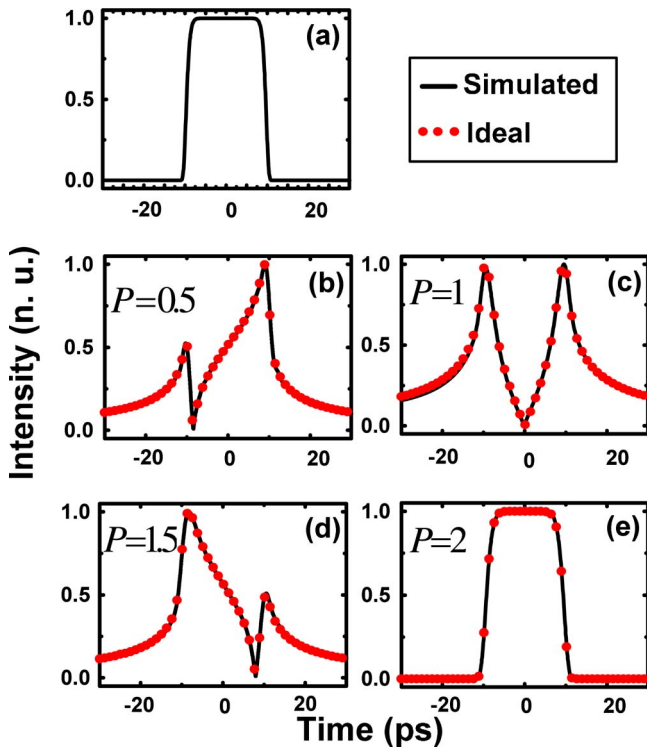
Fig. 4. (Color online) (a) Simulated temporal response of a photonic FHT for a fractional order of four different values. The envelope of the input optical signal and the envelope of the output signal for (b) $P=0.5$, (c) $P=1.0$, (d) $P=1.5$, and (e) $P=2.0$.

References

1. S. L. Hahn, in *The Transforms and Applications Handbook*, 2nd ed., A. D. Poularikas, ed. (CRC Press, 2000).
2. L. Venema, Nature Insight **424**, 809 (2003).
3. K. Tanaka, K. Takano, K. Kondo, and K. Nakagawa, in *Conference on Lasers and Electro-Optics* (Optical Society of America, 2001), Vol. 11, pp. 554–555.
4. H. Emami, N. Sarkhosh, L. A. Bui, and A. Mitchell, Opt. Lett. **33**, 98 (2008).
5. H. Emami, N. Sarkhosh, L. A. Bui, and A. Mitchell, Opt. Express **16**, 13707 (2008).
6. K. Tanaka, K. Takano, K. Kondo, and K. Nakagawa, Electron. Lett. **38**, 133 (2002).
7. M. Hanawa, K. Nakamura, K. Takano, and K. Nakagawa, in *Proceedings of the European Conference on Optical Communication* (VDE-Verlag, 2007), paper 01.5.6.
8. M. H. Asghari and J. Azaña, Opt. Lett. **34**, 334 (2009).
9. J. Azaña and L. R. Chen, J. Opt. Soc. Am. B **19**, 2758 (2002).
10. A. W. Lohmann, D. Mendlovic, and Z. Zalevsky, Opt. Lett. **21**, 281 (1996).
11. C. C. Tseng and S. C. Pei, IEEE Trans. Circuits Syst., II: Analog Digital Signal Process. **47**, 1529 (2000).
12. R. Feced, M. N. Zervas, and M. A. Muriel, IEEE J. Quantum Electron. **35**, 1105 (1999).
13. J. Skaar, L. Wang, and T. Erdogen, IEEE J. Quantum Electron. **37**, 165 (2001).
14. M. J. Cole, W. H. Loh, R. I. Laming, M. N. Zervas, and S. Barcelos, Electron. Lett. **31**, 1488 (1995).